BRL-TR-3184

FILE COPY

TECHNICAL REPORT BRL-TR-3184

BRL

AD-A230956

~~JAN 0 7 1991~~

JAN 8 1991

THEORETICAL STUDY OF THE RADIATIVE LIFETIME FOR THE SPIN-FORBIDDEN TRANSITION $a^3\Sigma_u^+ \rightarrow X^1\Sigma_g^+$ in He_2

CARY F. CHABALOWSKI
JAMES O. JENSEN
DAVID R. YARKONY
BYRON H. LENGSFIELD, III

DECEMBER 1990

APPROVED FOR PUBLIC RELEASE; DISTRIBUTION UNLIMITED.

U.S. ARMY LABORATORY COMMAND

BALLISTIC RESEARCH LABORATORY
ABERDEEN PROVING GROUND, MARYLAND

NOTICES

UNCLASSIFIED

REPORT DOCUMENTATION PAGE

Form Approved
OMB No. 0704-0188

1. AGENCY USE ONLY (Leave blank)

2. REPORT DATE
December 1990

3. REPORT TYPE AND DATES COVERED
Final, September 1986 - July 1988

4. TITLE AND SUBTITLE
Theoretical Study of the Radiative Lifetime for the Spin-Forbidden Transition $a^3\Sigma_u^+ \rightarrow X^1\Sigma_g^+$ in He_2.

5. FUNDING NUMBERS
PR: 1L161102AH43

6. AUTHOR(S)
Cary F. Chabalowski, *James O. Jensen, David R. Yarkony and Byron H. Lengsfield, III

7. PERFORMING ORGANIZATION NAME(S) AND ADDRESS(ES)

8. PERFORMING ORGANIZATION REPORT NUMBER

9. SPONSORING/MONITORING AGENCY NAME(S) AND ADDRESS(ES)
U.S. Army Ballistic Research Laboratory
ATTN: SLCBR-DD-T
Aberdeen Proving Ground, MD 21005-5066

10. SPONSORING/MONITORING AGENCY REPORT NUMBER
BRL-TR-3184

11. SUPPLEMENTARY NOTES
*James O. Jensen is an employee of the Chemical Research, Development, and Engineering Center, Aberdeen Proving Ground, MD.

12a. DISTRIBUTION/AVAILABILITY STATEMENT
Approved for public release, distribution unlimited.

12b. DISTRIBUTION CODE

13. ABSTRACT (Maximum 200 words)

The radiative lifetime for the spin-forbidden, dipole allowed transition $a^3\Sigma_u^+ \rightarrow X^1\Sigma_g^+$ in neutral He_2 was calculated. This transition is assumed to derive its intensity by spin-orbit (S-O) induced couplings which are treated using first-order perturbation theory. The first-order corrections to the wavefunctions are calculated directly in the configuration state function (CSF) basis by solving a set of linear equations given by first-order perturbation theory for the perturbation to the zeroth-order $X^1\Sigma_g^+$ and $a^3\Sigma_u^+$ wavefunctions. This approach eliminates the need to solve explicitly for many eigenstates of the unperturbed Hamiltonian which would be required if the spectral representation for the perturbed wavefunction were used. The results show a rapidly changing electric transition dipole moment as a function of internuclear separation, R(He-He), over the bound region of the $a^3\Sigma_u^+$ potential energy curve, i.e., R(He-He)-1.5 to 4.0 bohr. The transition dipole reaches a maximum near the small barrier to dissociation around R(He-He)=4.5 bohr. A vibrational analysis gives the lifetime of the v=0 level of $a^3\Sigma_u^+$ to be around 18 sec, which is consistent with a recent experimental estimate of 10 sec (v=?) as a lower bound.

14. SUBJECT TERMS
Helium, Radiative Lifetime, Quantum Chemistry

15. NUMBER OF PAGES
35

16. PRICE CODE

17. SECURITY CLASSIFICATION OF REPORT	18. SECURITY CLASSIFICATION OF THIS PAGE	19. SECURITY CLASSIFICATION OF ABSTRACT	20. LIMITATION OF ABSTRACT
UNCLASSIFIED	UNCLASSIFIED	UNCLASSIFIED	

NSN 7540-01-280-5500

Standard Form 298 (Rev 2-89)
Prescribed by ANSI Std Z39-18
298-102

UNCLASSIFIED

INTENTIONALLY LEFT BLANK.

TABLE OF CONTENTS

INTENTIONALLY LEFT BLANK.

LIST OF FIGURES

LIST OF TABLES

INTENTIONALLY LEFT BLANK.

1. INTRODUCTION

The generation of neutral excited state atoms or molecules in a liquid helium bath via collisions with alpha particles was initially reported by Surko and Reif (1968). Subsequent experiments utilizing discharges from beta emitters, again, submerged in liquid helium, also found a neutral entity in a long-lived excited state (Rayfield 1969; Mitchell and Rayfield 1971). This excited atom or molecule produced a He_2^+ ion and an electron at the liquid surface. It was suggested that this excited species was either the helium 2^3S atomic state or the $a^3\Sigma_u^+$ diatomic state which is known to be bound. Calvani, et al. (1972), generating the neutral entities from an alpha source, set a lower limit of 0.1 sec on its natural lifetime (τ).

A more recent experimental study by Mehrotra, Mann, and Dahm (1979), concluded that the neutral excited species was the $a^3\Sigma_u^+$ molecular state, i.e., the lowest energy excited state in He_2, and not the 2^3S atomic state. These workers predict a lower bound on the lifetime of 10 sec in liquid helium. This lifetime supports the assignment of the electronic state to the molecular $a^3\Sigma_u^+$ rather than the atomic 2^3S state which has an experimentally known lifetime of 15 μsec in the liquid helium (Mehrotra, Mann, and Dahm 1979).

Another interesting aspect of the excited molecule is that is reportedly forms a microscopic bubble in the liquid (Dennis et al. 1969; Hickman and Lane 1971) with a theoretically estimated diameter of 12.5 Å (Hansen and Pollock 1972). The size of the bubble is attributed to the size of the 2s Rydberg orbital comprising the He 2^3S state (Guberman and Goddard 1975).

In view of the large difference (a factor of 100) predicted by the two experiments (Calvani, Maraviglia, and Messana 1972; Calvani et al. 1974; Mehrotra, Mann, and Dahm 1979) for the lower limit of the lifetime of the $a^3\Sigma_u^+$ state in liquid helium, high quality *ab initio* calculations were undertaken in an effort to clarify this situation.

In this study, the lifetime, τ, for the spin-forbidden transition $a^3\Sigma_u^+ \rightarrow X^1\Sigma_g^+$ is obtained from calculations employing state averaged multiconfiguration SCF (MCSCF) plus configuration interaction (CI) wavefunctions to describe the appropriate zeroth-order states. In order to calculate this spin-forbidden lifetime, the spin-orbit (S-O) induced perturbation Ψ^1 to each zeroth-order state will be calculated using the full microscopic Breit-Pauli Hamiltonian (Bethe and Salpeter 1977). A recently

implemented method (Yarkony 1986, 1987) which employs the symbolic matrix element approach of Liu and Yoshimine (1981) in the evaluation of the S-O matrix elements will be used to evaluate the Ψ^1 directly from a system of linear equations in the configuration state function (CSF) basis. This technique has been used successfully for studying spin-forbidden transitions in other molecules (Yarkony 1986, 1987).

2. METHODS

The CI method used to obtain the zeroth-order wavefunctions is the symbolic matrix element, direct-CI method of Liu and Yoshimine (1981). The molecular orbitals (MOs) needed as a basis set for the CI expansions were obtained from a state-averaged multiconfiguration self consistent field (SA-MCSCF) approach. The SA-MCSCF procedure is the general second-order, density matrix driven MCSCF algorithm of Lengsfield (1982). From the SA-MCSCF procedure one obtains a set of molecular orbitals determined by minimizing the energy functional

$$E_{avg} = \sum_k w_k < \Psi_k^o | H^o | \Psi_k^o > = \sum_k w_k \, E_k \tag{1}$$

where the Ψ_k^o's are the eigenfunctions of H^o, the non-relativistic Hamiltonian operator, in the space of the MCSCF expansion

$$\Psi_k^o = \sum_i c_i^k \psi_i \, . \tag{2}$$

Above, the w_k's are the non-negative weighing factors for the electronic states which do not vary as a function of internuclear separation, and the ψ_i are the CSFs composed of the state-averaged, optimized MOs. The weights were chosen to provide a balanced description of the states of interest. The sensitivity of the multi-reference CI results to a particular choice of w_k's in the MCSCF optimization was tested by varying the weights and by comparing our results to both experimentally derived spectroscopic parameters and to spectroscopic parameters obtained in earlier *ab initio* calculations which employed a separate MCSCF procedure for each state (Konowalow and Lengsfield 1987a, 1987b).

2.1 Spin-Orbit Interactions.

The spin-orbit part, H^{so}, of the microscopic Breit-Pauli interaction is given by (Bethe and Salpeter 1977)

$$H^{so} = \frac{e}{2mc^2}\left[\sum_{i,K}\frac{Z_K}{r_{Ki}^3}\;\vec{l_i}(K)\cdot\vec{s_i} - \sum_{i\neq j}\left(\frac{\vec{r_{ij}}\;x\;\vec{p_i}}{r_{ij}}\right)\cdot(\vec{s_i}+2\vec{s_j})\right]. \tag{3}$$

Due to helium's small nuclear charge, the S-O interactions are expected to be small and, therefore, well suited for treatment by first order perturbation theory. The total perturbed wavefunction for state I is given by

$$\Psi_I = \Psi_I^o + \Psi_I^1 , \tag{4}$$

with Ψ_I^o being the zeroth-order wavefunction. The usual spectral representation for the first-order correction Ψ_I^1 due to S-O effects is

$$\Psi_I^1 = \sum_{J\neq I}^{L}\frac{\langle\Psi_J^o|H^{so}|\Psi_I^o\rangle}{(E_I^o - E_J^o)}\,\Psi_J^o . \tag{5}$$

The summation over the L electronic states is, in principle, infinite. One often used approach to solving for Ψ_I^1 is to calculate explicitly the wavefunctions for a relatively small number of excited states thereby drastically truncating L. This might cause one to miss important contributions to Ψ_I^1 from the omitted states.

Within a given CSF space, this "omitted states" problem is eliminated by solving for Ψ_I^1 directly from

$$(H^o - E)\,\Psi_I^1 = -H^{so}\Psi_I^o . \tag{6}$$

Equation 6 can be transformed into matrix form as

$$(\underset{\approx}{H^o} - E)\underset{\sim}{V^I} = -\underset{\approx}{H^{so}}\;\underset{\sim}{C^I} \tag{7}$$

where it must be emphasized that $\underset{\approx}{H^o}$ and $\underset{\approx}{H^{so}}$ are matrices with elements formed over CSFs, not over eigenstates. The vectors $\underset{\sim}{V^I}$ and $\underset{\sim}{C^I}$ are defined as the coefficients for the first- and zeroth-order parts of Ψ_I:

$$\Psi_I^o = \sum_i C_i^I\;\psi_i(\kappa) \tag{8a}$$

$$\Psi_I^1 = \sum_j V_j^I\;\psi_j(\kappa') . \tag{8b}$$

The κ and κ' label the spatial symmetries to which the CSFs belong, and in general, $\kappa \neq \kappa'$. Equation 7 forms a large set of linear inhomogeneous equations which are solved to obtain $\underset{\sim}{V}$ by a variant of the method suggested by Pople, et al (1979).

2.2 Perturbed Wavefunctions. The following perturbations to $\Psi^o(X^1\Sigma^+_{go+})$ and $\Psi^o(a^3\Sigma^+_{u1})$ are calculated

$$\Psi\ (X^1\Sigma^+_{go+}) = \Psi^o(X^1\Sigma^+_{go+}) + \Psi^1(^3\Pi_{go+};X^1\Sigma^+_{go+}) \tag{9a}$$

$$\Psi\ (a^3\Sigma^+_{u1}) = \Psi^o(a^3\Sigma^+_{u1}) + \Psi^1(^1\Pi_{u1};a^3\Sigma^+_{u1}) \tag{9b}$$

where the first-order corrections arise from the S-O interactions

$$\Psi^1(^3\Pi_{go+};X^1\Sigma^+_{go+}) : < {}^3\Pi_{go+}|H^{so}|X^1\Sigma^+_{go+} > \Omega = 0^+$$

$$\Psi^1(^1\Pi_{u1};a^3\Sigma^+_{u1}) : < a^3\Sigma^+_{u1}|H^{so}|^1\Pi_{u1} > \Omega = 1\ .$$

Where the quantum number Ω ($\Omega = \Lambda + S_z$), the z-component of the total orbital and spin angular momentum is conserved. Below, the first-order wave-functions will be abbreviated as $\Psi^1(^3\Pi_{go+})$ and $\Psi^1(^1\Pi_{u1})$.

2.3 Electronic Transition Dipole Moment. In order to calculate the lifetime of the $a^3\Sigma^+_u \rightarrow X^1\Sigma^+_g$ transition, the electric transition dipole moment $\mu_1(a^3\Sigma^+_u,X^1\Sigma^+_g)$, defined by

$$\mu_1(a^3\Sigma^+_u,X^1\Sigma^+_g) = < \Psi\ (a^3\Sigma^+_{u1})\ |\mu_{+1}|\Psi\ (X^1\Sigma^+_{go+}) > \tag{10}$$

is required. The quantity, μ_{+1}, is the shift operator form of the total electric dipole moment operator which has components $(\mu_{+1},\mu_{-1},\mu_o)$. Substituting the perturbation expansion for each state in Equation 10 gives, to first-order,

$$\mu_1(a^3\Sigma_u^+,X^1\Sigma_g^+) = <\Psi^o(a^3\Sigma_{u1}^+)|\mu_{+1}|\Psi^1(^3\Pi_{go+})> + <\Psi^1(^1\Pi_{u1})|\mu_{+1}|\Psi^o(X^1\Sigma_{go+}^+)>. \tag{11}$$

Since the lower state in this transition is largely repulsive (possessing only a very shallow van der Waals well), we need to obtain the vibrationally averaged transition dipole moment between a bound electronic state (here the $a^3\Sigma_u^+$) with vibrational wavefunction $\chi_{v'}(R)$ and a repulsive state (here the $X^1\Sigma_g^+$ state) with a continuum vibrational wavefunction $\chi_{k''}(R)$ is

$$S_{v'k''} = <\chi_{v'}(R)|\mu_1(a^3\Sigma_u^+,X^1\Sigma_g^+)|\chi_{k''}(R)> \tag{12}$$

where k'' represents the energy for the continuum state (van Dishoeck, Langhoff, and Dalgarno 1983; van Dishoeck and Dalgarno 1983). $\chi_k''(R)$ and $\chi_v'(R)$ are obtained by numerically solving the radial Schroedinger equation for nuclear motion while ignoring rotational effects. The vibrational wavefunction for the bound state is normalized to unity and the continuum wavefunction is defined by

$$\chi_k(R) = \left(\frac{2\mu}{\pi k}\right)^{1/2} \sin(kR-n) \tag{13}$$

where n is a phase shift factor and μ the reduced mass of He_2.

The Einstein coefficient for spontaneous emission from the v' to the k'' vibrational state is (van Dishoeck, Langhoff, and Dalgarno 1983; van Dishoeck and Dalgarno 1983):

$$A_{v'k''} = (2.1419x10^{10})\cdot\Delta E^3(au)\cdot|S_{v'k''}|^2 \ . \tag{14}$$

The radiative lifetime for the v' level is obtained by integrating Equation 14 over k''.

3. DETAILS OF CALCULATIONS

The Gaussian-type basis set is essentially that used by Sunil, et al. (1983) in an earlier theoretical study on the excited states of He_2 with two exceptions. A single, primitive p function has been added with its exponent optimized in increments of 0.001 to give the lowest energy for the $F^1\Pi_u$ at R = 2.00

bohr (i.e., near r_e). The CI part of the optimization used MOs obtained from a MCSCF calculation on the $F^1\Pi_u$ state (i.e., no state averaging). This additional p function was deemed necessary due to an unacceptably large $\Delta E(F^1\Pi_u - a^3\Sigma_u^+)$ at R = 2.00 bohr when compared with the experimental T_e between these two states. The orbital exponent for the more diffuse d-function was also changed to be consistent with a basis set used in an earlier study on He_2 conducted in this laboratory (Konowalow and Lengsfield 1987a, 1987b). The final atomic basis set, reproduced in Table 1, consists of (10s,6p,2d) primitives contracted to (7s,5p,2d), for a total of 34 atomic basis functions per atom.

The calculations are performed in D_{2h} symmetry with the appropriate averaging of states in the SA-MCSCF to give wavefunctions which transform according to $D_{\infty h}$ symmetry. In D_{2h}, the states transform according to the irreducible representations (IRREPs) $X^1\Sigma_g^+(^1A_g)$, $a^3\Sigma_u^+(^3B_{1u})$, $b^3\Pi_g(x{:}^3B_{2g}, y{:}^3B_{3g})$, and $F^1\Pi_u(x{:}^1B_{3u}, y{:}^1B_{2u})$.

The SA-MCSCF is of the CAS type wherein the four electrons are distributed, in all possible ways, amongst the lowest three MOs from IRREPs $a_g(\sigma_g)$ and $b_{1u}(\sigma_u)$, and the lowest MO from $b_{2u}(\pi_{uy})$, $b_{3u}(\pi_{ux})$, $b_{2g}(\pi_{gx})$, and $b_{3g}(\pi_{gy})$, consistent with space and spin symmetry restrictions. The state averaged energy is then optimized according to Equation 1, including the states $X^1\Sigma_g^+$, $a^3\Sigma_u^+$, $b^3\Pi_{gx}$, $b^3\Pi_{gy}$, $F^1\Pi_{ux}$, and $F^1\Pi_{uy}$. Two different weighing schemes were used in this study. The weights $\underset{\sim}{w}$ = (2, 2, 1, 1, 1, 1), and $\underset{\sim}{w}$ = (1.5, 1.5, 1, 1, 1, 1) were employed and are denoted as Scheme 1 and Scheme 2, respectively.

The energy was found to be consistent for the two sets of weights to $\leq 1.\mathrm{x}10^{-5}$ Hartrees and the electric transition dipole moments (for $X^1\Sigma_g^+ \leftarrow a^3\Sigma_u^+$) differed by less than 1%. An additional check on the choice of weighing factors comes from the comparison of the computed molecular constants with the experimental values (see Table 4) when available. Finally, comparison of the results for the $a^3\Sigma_u^+$ state from this study with extensive non-state averaged calculations of Konowalow and Lengsfield (1987b) shows good agreement for the r_e, D_e, ω_e, and the description of the "intermediate hump" in the potential energy curve (PEC) for this state.

At smaller internuclear separations (R = 1.3, 1.5, 1.6), the basis set became linearly dependent and molecular orbitals were eliminated in order to obtain convergence in the CI diagonalization. At R(He - He) = 1.30, one MO of b_{1u} symmetry was eliminated from the virtual space, and at R = 1.50 and 1.60, two MOs of b_{1u} symmetry were eliminated. These correspond to MOs consisting primarily of the most diffuse s-type atomic orbital (AOs).

The effect of eliminating these MOs was checked at R = 1.70 by comparing the results for calculations with all MOs included to calculations where first one MO and then a second MO was removed (in decreasing order of diffuseness) from the b_{1u} IRREP. It was found that by eliminating one MO, and then a second, the energy differed by no more than $\pm 3 \times 10^{-5}$ Hartree for any state when compared to the calculation using all the MOs. The transition dipole moment differed by no more than 3%. The vibrational analysis was re-run with the electric transition moment increased at these three points by twice the variation witnessed at R = 1.70 (i.e., by a factor of .06), then again with the transition moment decreased by a factor of .06 at these points. All the resulting lifetimes were identical to the initial results to within at least two significant digits. Stability in the lifetimes to this level of precision is acceptable for this study.

The final zeroth-order wavefunctions were obtained from second-order CIs with respect to the SA-MCSCF active space. The size of the resulting CI expansion (in number of CSFs) for each state is $X^1\Sigma_g^+$(27,381), $a^3\Sigma_u^+$(38,218), $b^3\Pi_g$(33,702), $F^1\Pi_u$(23,490), for the cases where no MOs were eliminated. When one and two MOs of b_{1u} symmetry were eliminated, the corresponding totals are (26,364, 36,794, 32,607, 22,736) and (25,369, 35,403, 31,530, 21,992), respectively.

In the vibrational analyses, PECs were represented by spline functions over the region for which ab initio data was available with extrapolation using Lennard-Jones 6-12 functional forms. The $a^3\Sigma_u^+$, $b^3\Pi_g$, and $F^1\Pi_u$ states were represented by spline functions for the region R = 1.30 - 6.50 bohr, while spline functions were used to represent the $X^1\Sigma_g^+$ PEC for the region R = 1.30 - 15.0 bohr. The total electric dipole transition moment was also represented by a spline function for points along R = 1.3 - 6.5 bohr, and described by a second-order polynomial outside this range.

4. RESULTS AND DISCUSSION

4.1 Stale Properties. One finds the following state description at R = 2.00 bohr:

$X^1\Sigma_g^+$: $1\sigma_g^2 1\sigma_u^2$

$a^3\Sigma_u^+$: $1\sigma_g^2 2\sigma_g 1\sigma_u$

$b^3\Pi_g$: $1\sigma_g^2 1\sigma_u 1\pi_u$

$F^1\Pi_u$: $1\sigma_g^2 1\sigma_u 1\pi_g$

Much of the behavior in the bound region can be understood by treating He_2^* as He_2^+ plus an electron in a Rydberg orbital. The three electrons of He_2^+ form the tightly bound "core" electrons (with MO occupation $1\sigma_g^2 1\sigma_u$) which interact to form the attractive potential at small R values. All three excited states have this core description in the dominant CSF within the bound region. For R > 3.0 bohr, the contribution from a CSF containing the anti-bonding configuration $1\sigma_g 1\sigma_u^2$ begins to make a significant contribution for the three excited states in this study. Figure 1 contains plots of the potential energy curves (PECs) for the four states of interest, and Table 2 reports the actual energies. Table 4 compares the spectroscopic constants for the four states of interest as predicted by this study and experiment. These are provided, in part, as a check on the overall quality of the wavefunctions used in this study. The theoretical D_e values are calculated as the difference in energy $E(r_e)$ - E(R = 40 bohr), with $E(r_e)$ determined from a three-point fit to a parabola.

Table 5 lists the lowest 10 vibrational levels for $a^3\Sigma_u^+$ state as calculated from the vibrational analysis. The v = 9 level lies 13,332 cm^{-1} above the equilibrium energy and 2,848 cm^{-1} below the barrier maximum. Table 5 also includes the v = 0 - 9 levels for the $b^3\Pi_g$ and the v = 0 - 3 for the $F^1\Pi_u$.

In the following sections, an analysis of the $a^3\Sigma_u^+$, $F^1\Pi_u$, and $b^3\Pi_g$ states of He_2 is presented. A general discussion of the structure of the wavefunctions for the excited states of He_2^* and its relationship to the shape of the PECs can be also found in papers by Mulliken (1964a, 1964b, 1966), and by Guberman and Goddard (1975), who place special emphasis on the Σ states.

4.1.1 The $a^3\Sigma_u^+$ State. The small barrier to dissociation, or "hump", has a maximum in this study at R = 2.70Å, and is reported (Jordan, Siddigui, and Siska 1986; Milliken 1964b) to occur from the competition between the attractive ionic-like core and the long-range repulsive interaction. Table 3 gives various estimates of this barrier. The present study calculates the barrier height to be 1.56 kcal/mol at 2.70Å, which agrees well with the relatively recent experimental value of 1.43±.05 kcal/mol at 2.72±.04Å reported by Jordan, Siddigui, and Siska (1986). Probably the best theoretical estimate (and maybe the best overall estimate) for this barrier comes from a recent paper by Konowalow and Lengsfield (1987) who calculate the barrier to lie at 2.712Å with a height of 1.507 kcal/mol. These agree quite well with the values obtained in the current study. As can be seen in Table 4, the calculated r_e, ω_e, T_e, and D_e vary from experiment by no more than 1%.

4.1.2 The $F^1\Pi_u$ State. The existence of the barrier with a predicted maximum of 10.9 kcal/mol at R = 1.79Å has been shown to arise primarily from an avoided crossing with a higher state of the same $^1\Pi_u$ symmetry, particularly the interaction with the state that dissociates to He($1s^2$) + He*(1s3d) (Gupta and Matson 1969). Mulliken (1964a, 1966) also predicted the existence of a barrier due to a change-over of the $F^1\Pi_u$ state from one which looks like a 3dΠ state in the united atom orbital (UAO) description to one with $1s^2$ + 1s2p character as it approaches the dissociation limit.

Table 3 compares the current values for the height (10.9 kcal/mol) and location (R_{max} = 1.79Å) of this barrier with results from two other theoretical studies. Gupta and Matsen (1969) calculated values of 13.5 kcal/mol and 1.73Å for the barrier height and location, while Browne's (1965) results predict 12.5 kcal/mol at 1.77Å. The predicted location for the maximum from these three studies are in reasonable accord. It is not surprising however, that the barrier height calculated in this study (i.e., 10.9 kcal/mol) differs significantly from these other, very early calculations.

The calculated r_e, ω_e, and T_e for this state are in good accord with the experimental values (see Table 4). No experimental D_e was reported. It should be pointed out that the $b^3\Pi_g$ and $F^1\Pi_u$ states do not enter independently into our calculations of the $a^3\Sigma_u^+ \rightarrow X^1\Sigma_g^+$ transition moment, since the contributions from a large number of states of a particular symmetry are obtained by solving for the perturbation over CSFs. However, it is still important that the CSF lists and MOs provide a suitable basis for describing the $^1\Pi_u$ and $^3\Pi_g$ spaces, and so a comparison of the theoretical and the experimental spectroscopic constants provides a useful check of our calculations.

4.1.3 The $b^3\Pi_g$ State. The $b^3\Pi_g$ has a UAO description of 2pΠ which dissociates to He($1s^2$) + He*(1s2p), thus Mulliken predicted that a hump is not likely to occur in the PEC for this state since it is not a "promoted" Rydberg MO state. The potential energy curve for the $b^3\Pi_g$ state shown in Figure 1 does not indicate a barrier, thus supporting this prediction.

Table 4 shows the calculated r_e, ω_e, and T_e, to again be in excellent agreement with the available experimental values. No experimental D_e is reported.

4.2 Transition Properties.

4.2.1 Spin-Orbit Interactions. The first-order corrections to the $X^1\Sigma_g^+$ and $a^3\Sigma_u^+$ states arise from interactions of these zeroth-order wavefunctions with the $^3\Pi_g$ and $^1\Pi_u$ symmetry manifolds, respectively. The magnitude of the perturbation of the $a^3\Sigma_u^+$ by the $^1\Pi_u$ manifold is plotted in Figure 2a, and labeled Curve A. Curve B in Figure 2a represents the first-order SO perturbation of the $a^3\Sigma_u^+$ zeroth-order wavefunction attributable to only the lowest energy state of $^1\Pi_u$ symmetry, the $F^1\Pi_u$ state. That is the L=1 trunction of Equation 5. Therefore, the difference between Curves A and B reflects the error in the first-order perturbation treatment of $\Psi^o(a^3\Sigma_{u1}^+)$ that is being introduced by truncating the summation in Equation 5 to simply L=1. The analogous information is plotted in Figure 2b for the $X^1\Sigma_g^+$ state being perturbed by the $^3\Pi_g$ manifold (Curve A) or only the $b^3\Pi_g$ state (Curve B).

One can immediately see that much of the contribution to the total perturbation is excluded from the Ψ^1's if only the interaction with the lowest energy $^1\Pi_u$ or $^3\Pi_g$ state is included. The difference in the contributions at R=2.00 is a factor of ten for the $a^3\Sigma_{u1}^+$ - $^1\Pi_{u1}$ SO interaction and more than a factor of 20 for the $X^1\Sigma_{go+}^+$ - $^3\Pi_{go+}$ interaction. The discrepancies change near R=4.0 bohr, where the perturbation of the $a^3\Sigma_u^+$ state by a single $^1\Pi_u$ state accounts for approximately 79% of the total interaction attributed to the $^1\Pi_u$ manifold. However, the single-state approximation for the $X^1\Sigma_{go+}^+$ - $^3\Pi_{go+}$ perturbation is more than one hundred-fold less than that calculated from the interaction with the entire $^3\Pi_g$ manifold for most of the bound region.

4.2.2 Electric Transition Dipole Moment and Lifetimes. The total electric transition dipole moment, $\mu_1(a^3\Sigma_u^+,X^1\Sigma_g^+)$, obtained from the perturbed wavefunctions in Equations 9, as well as its singlet and triplet components (as given in Equation 11), are plotted as the dotted curves in Figure 3, and Table 6 lists the values of $\mu_1(a^3\Sigma_u^+,X^1\Sigma_g^+)$ as a function of R(He-He). It can be seen that the singlet component dominates over most of the $a^3\Sigma_u^+$ bound potential, with the triplet component having comparable magnitude only at small internuclear separations. At R=1.6, the triplet component is already a factor of five smaller than the single contribution.

The two moments have opposite signs for values less than 2.0 bohr, and then have the same sign up through R=3.5, where the signs are once again opposites. The difference is signs at small internuclear separation causes a cancellation in forming the total transition moment, generating a near

zero moment at R=1.50 bohr. From R≥1.85, the total transition dipole is largely determined by the singlet component which has a maximum value of 6.0×10^{-6} au at R=3.8 (from fitting to a parabola). The decreasing transition moment for large R is consistent with the separated atom limit, for which the electric transition dipole moment must go to zero as it represents a $He(^3s_g) \rightarrow He(^1s_g)$ transition.

The single state L=1 approximation in Equation 5 is also considered in Figure 3. The solid curves in Figure 3 provide the singlet and triplet components, as well as the total $\mu_1(a^3\Sigma_u^+,X^1\Sigma_g^+)$ as given in Equation 11, but calculated within the L=1 approximation. Comparing the dotted curves with the solid curves one finds at least three main differences. First, the singlet contribution to $\mu_1(a^3\Sigma_u^+,X^1\Sigma_g^+)$ for the single-state perturbation (SSP) (solid curve) is essentially zero for the region R=1.3 to 2.6 bohr, in sharp contrast to the singlet contribution given by the dotted curve, which never falls below 50% of the maximum in $\mu_1(a^3\Sigma_u^+,X^1\Sigma_g^+)$. The second observation is that the triplet contribution to $\mu_1(a^3\Sigma_u^+,X^1\Sigma_g^+)$, from the SSP is much larger in this region. For example, at 1.85 bohr, the triplet contribution is -2.1×10^{-6} au for the SSP, while it is essentially zero for the perturbation over the manifold of states. The third feature is the relative magnitude of the total $\mu_1(a^3\Sigma_u^+,X^1\Sigma_g^+)$'s near their maxima. For example, at R=4.0 bohr, we find $\mu_1(a^3\Sigma_u^+,X^1\Sigma_g^+)=6.0 \times 10^{-6}$ au for the calculation over the $^1\Pi_u$ manifold, while the SSP gives $\mu_1(a^3\Sigma_u^+,X^1\Sigma_g^+)=3.5 \times 10^{-6}$ au, and therefore accounts for only 58% of the predicted total magnitude of the transition dipole moment. However, from Figure 2a, we see that at this geometry approximately 79% of the S-O perturbation is accounted for using the SSP. Thus, the electric transition dipole moment converges more slowly with respect to L, the number of excited states included in Equation 5, than the S-O first-order perturbation contribution to $\Psi(a^3\Sigma_{u1}^+)$.

Table 5 lists the predicted lifetimes and energies from this study for the v=0-9 vibrational levels of the $a^3\Sigma_u^+$ state for a radiative decay process to the repulsive $X^1\Sigma_g^+$ state. The predicted lifetime for the v=0 level is 18 sec, which is consistent with the more recent experimental prediction of 10 sec (v=unknown) for a lower bound in liquid helium. The lifetimes are seen to monotonically decrease with increasing vibrational quantum number, at least up to v=9. At v=5, the lifetime falls below the predicted lower bound of 10 sec. The calculated lifetime of the v=0 level using the electric transition dipole moment represented by the solid curve in Figure 3 (from the single state approximation to Equation 5), is predicted to be 195 sec, in sharp contrast with results determined by including all of the eigenstates in our CSF basis.

5. CONCLUSIONS

The lifetime for the He_2 $a^3\Sigma_u^+$ excited state is predicted to be 18 sec for the v=0 vibrational level in the gas phase, supporting the experimental value for the lower bound (in condensed phase) offered by Mehrotra, et al. (1979), of 10 sec. These calculations also predict the lifetime to decrease continuously with increasing vibrational quantum number, at least up to the v=9 vibrational state.

One finds that the $\mu_1(a^3\Sigma_u^+,X^1\Sigma_g^+)$ shows maxima near 4 bohr, and the electric transition dipole moment for internuclear separations greater than 1.60 bohr is determined almost entirely by the singlet component, $<\Psi^1(^1\Pi_{u1}:a^3\Sigma_{u1}^+)|\mu_{+1}|\Psi^o(X^1\Sigma_{go+})>$. S-O interactions originating in $^1\Pi_u$ states beyond the $F^1\Pi_u$ are essential to the characterization of the $\Psi^1(^1\Pi_{u1}:a^3\Sigma_{u1}^+)$ wavefunction, as well as $\mu_1(a^3\Sigma_u^+,X^1\Sigma_g^+)$. This is a strong argument in favor of using the method employed in this study, which is designed specifically to include these higher energy contributions at little or no additional cost.

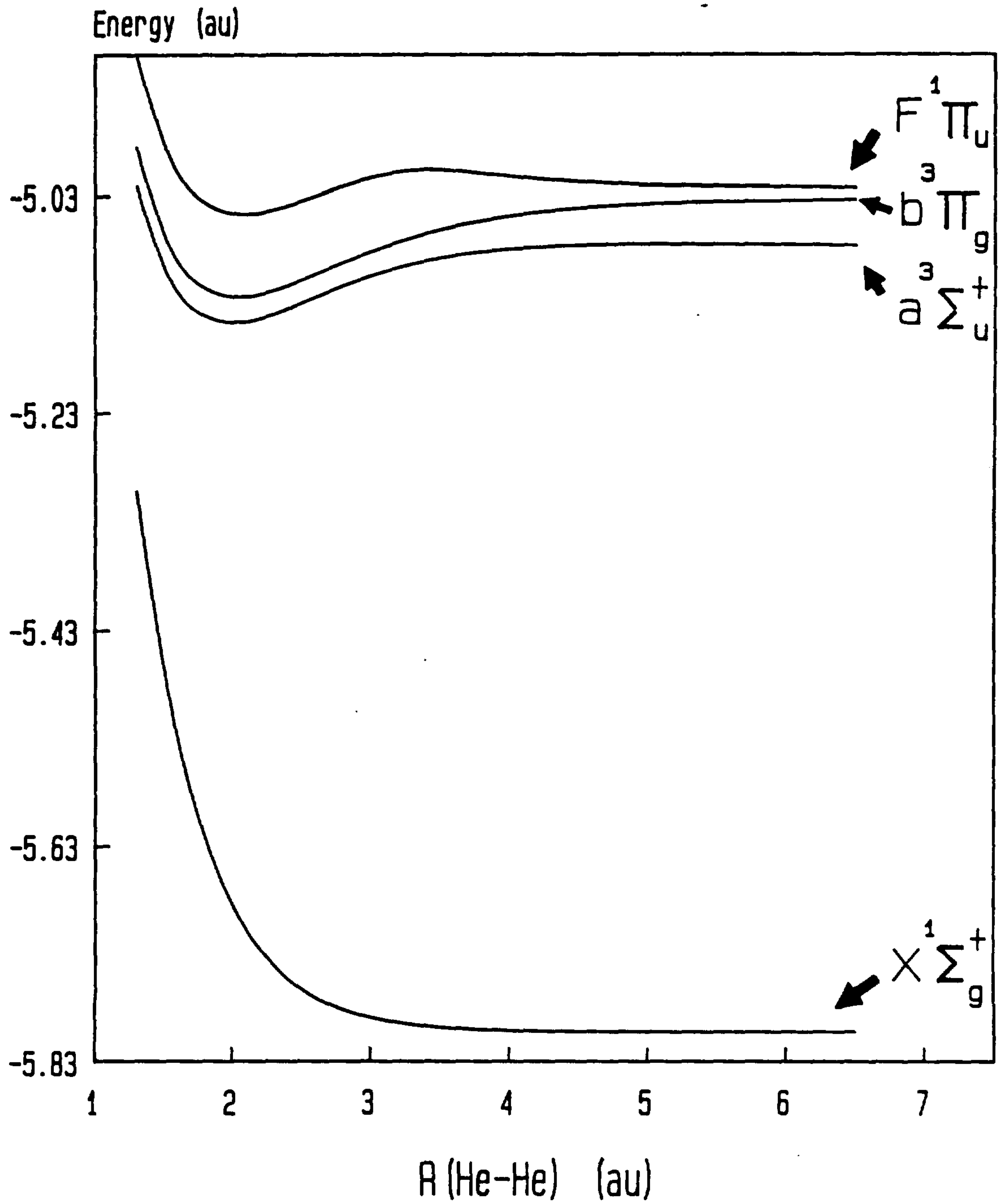

Figure 1a. Potential Energy Curves for the $X^1\Sigma_g^+$, $a^3\Sigma_u^+$, $b^3\Pi_g$, and $F^1\Pi_u$ Electronic States in He_2.

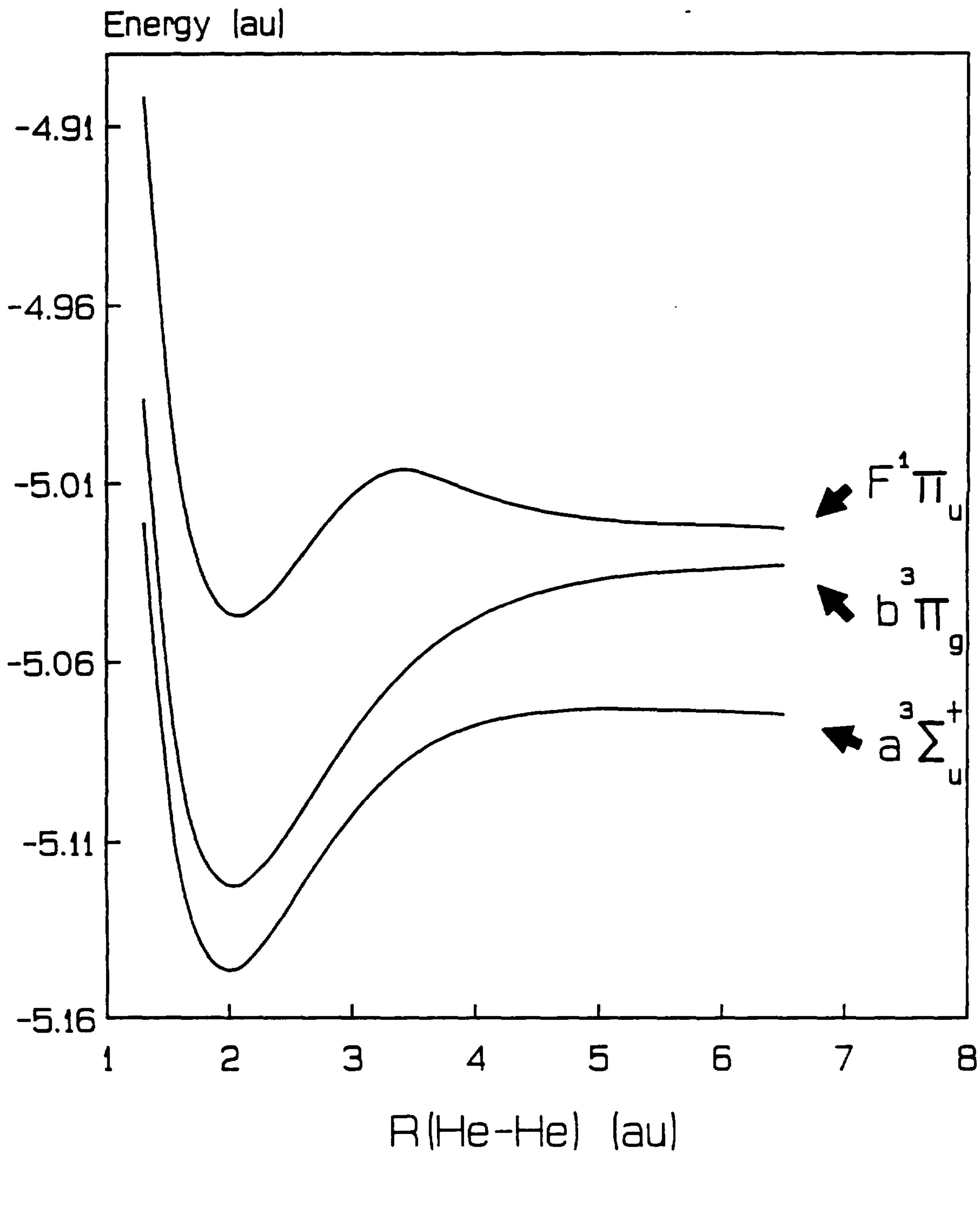

Figure 1b. Blow-up of the Potential Energy Curves for the $a^3\Sigma_u$, $b^3\Pi_g$, and $F^1\Pi_u$ States.

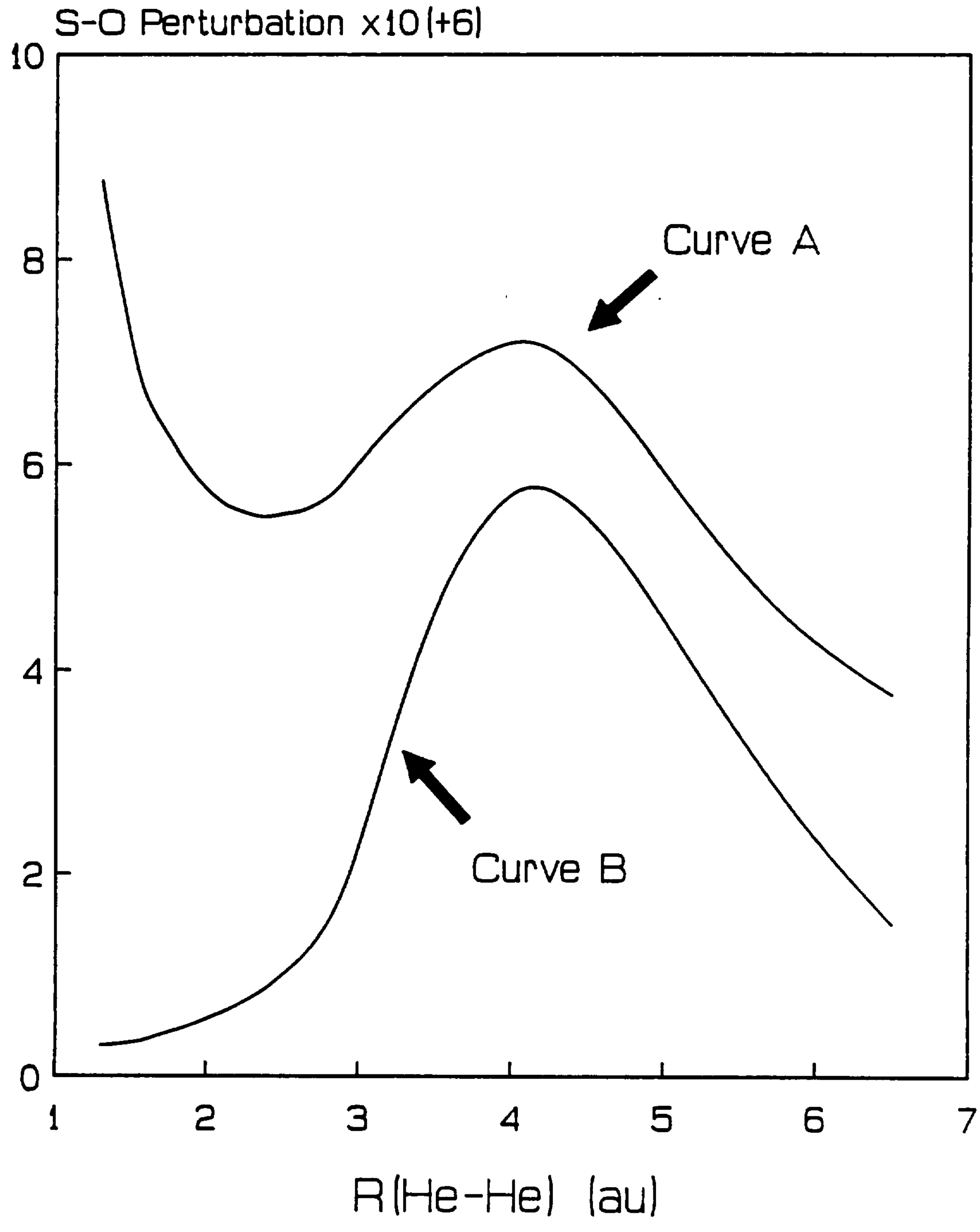

Figure 2a. First-Order Contribution to the Spin-Orbit Perturbation of the $a^3\Sigma_u^+$ by the $^1\Pi_u$ State Manifold (Curve A) and by the $F^1\Pi_u$ State (Curve B).

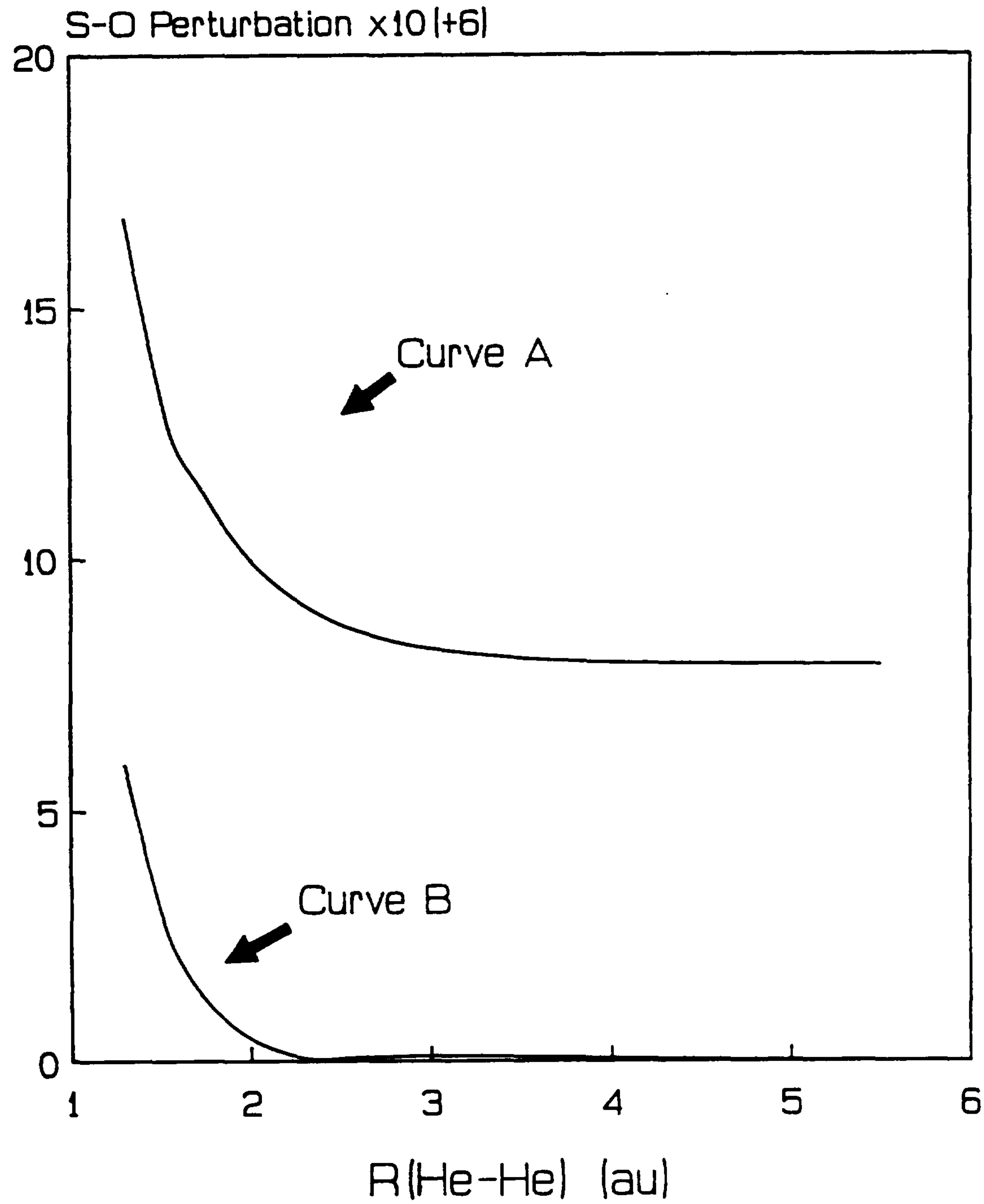

Figure 2b. First-Order Contribution to the Spin-Orbit Perturbation of the $X^1\Sigma_g^+$ by the $^3\Pi_g$ State Manifold (Curve A) and by the $b^3\Pi_g$ State (Curve B).

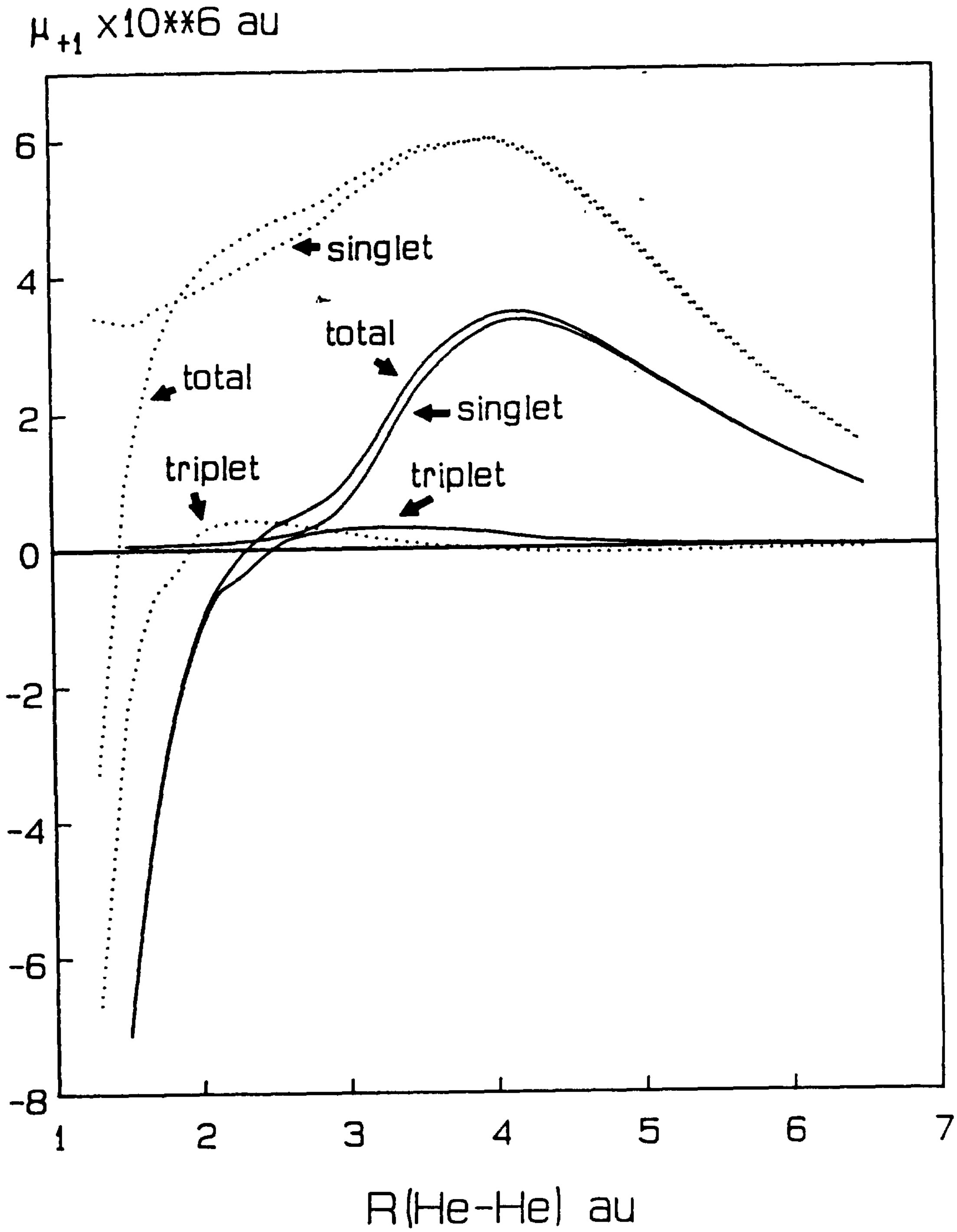

Figure 3. (...): Total Electric Dipole Transition Moment and Singlet and Triplet Components Using Perturbed Wavefunctions Including the SO Interactions with the Entire $^1\Pi_u$ and $^3\Pi_g$ State Manifolds. (---); Electric Dipole Transition Moment and Components for the Single-state Perturbed Wavefunctions Having SO Interactions With Only the $F^1\Pi_u$, and $b^3\Pi_g$.

Table 1. Atomic Basis Set

Type	Exponent	Coefficient
s	501.5045	0.002498
	75.31147	0.019099
	17.20769	0.092978
	4.886925	0.311074
	1.569584	1.0
	0.541551	1.0
	0.193932	1.0
	0.104560	1.0
	0.026725	1.0
	0.008017	1.0
p	10.19643	0.092050
	2.414857	0.474058
	0.746691	1.0
	0.139276	1.0
	0.032392	1.0
	0.012	1.0
d	1.5	1.0
	0.042	1.0

Table 2. CI State Energies as a Function of R(He-He)[a]

r(He-He)	$X^1\Sigma_g^+$	$a^3\Sigma_u^+$	$b^3\Pi_g$	$F^1\Pi_u$
1.30	-5.302222	-5.021207	-4.986410	-4.901985
1.50	-5.469882	-5.098117	-5.067915	-4.986402
1.60	-5.532127	-5.119922	-5.091493	-5.011180
1.70	-5.583158	-5.134085	-5.107148	-5.027931
1.85	-5.642728	-5.144880	-5.119785	-5.042067
1.90	-5.658859	-5.146409	-5.121831	-5.044584
2.00	-5.686530	-5.147189	-5.123516	-5.047177
2.10	-5.709037	-5.145601	-5.122740	-5.047252
2.15	-5.718626	-5.144177	-5.121637	-5.046572
2.30	-5.741993	-5.138132	-5.116346	-5.042518
2.40	-5.753907	-5.133160	-5.111710	-5.038691
2.50	-5.763483	-5.127971	-5.106540	-5.034360
2.60	-5.771267	-5.122332	-5.101183	-5.029804
2.70	-5.777500	-5.166891	-5.095719	-5.025212
2.85	-5.784629	-5.109085	-5.087677	-5.018643
3.00	-5.789709	-5.102519	-5.080019	-5.012907
3.25	-5.795223	-5.092835	-5.068858	-5.006811
3.40	---[b]	---	---	-5.005982
3.50	-5.798365	-5.085661	-5.059869	-5.006494
3.70	-5.799860	-5.081535	-5.054116	-5.008882
4.00	-5.801126	-5.077456	-5.047474	-5.013024
4.25	-5.801675	-5.075460	-5.043445	-5.015822
4.50	-5.801973	-5.074317	-5.040475	-5.017919
4.75	-5.802132	-5.073739	-5.038312	-5.019440
5.00	-5.802214	-5.073526	-5.036750	-5.020526
5.25	-5.802254	-5.073542	-5.035628	-5.021295
5.50	-5.802272	-5.073692	-5.034824	-5.021838
6.00	-5.802279	-5.074169	-5.033841	-5.022489
6.50	-5.802275	-5.074671	-5.033337	-5.022815
10.00	-5.802260	-5.075958	-5.032746	-5.023218
40.00	-5.802255	-5.075983	-5.032699	-5.023338

[a] Atomic units used throughout.

[b] Calculated only the $F^1\Pi_u$.

Table 3. Barrier Heights and Barrier Positions for the $a^3\Sigma_u^+$ and $F^1\Pi_u$ States

State	This Study Height[a]	This Study Position[b]	Previous Theory Height	Previous Theory Position	Experiment Height	Experiment Position
$a^3\Sigma_u^+$	1.56	2.70	2.7 1.85 1.507	2.9[c] 2.68[d] 2.712[j]	1.82[e] 1.55 1.43±.05	2.77[f] 2.72±.04[g]
$F^1\Pi_u$	10.9	1.79	13.5 12.5[i]	1.73[h] 1.78[i]		

[a] Energies in kcal/mol.
[b] Distances in Angstroms.
[c] Peach (1978).
[d] Sunil et al. (1983), MCSCF calculations.
[e] Lundlum, Larson, and Caffrey (1967)
[f] Brutschy and Haberland (1979).
[g] Jordan, Siddiqui, and Siska (1986).
[h] Gupta and Matsen (1969), Valence-bond calculations.
[i] Browne (1965) did not report a barrier position from any fitting procedure, so we calculated the position and height by fitting the potential energy data in Table 1 of Browne (1965) to a parabola giving these results.
[j] Large-scale MCSCF plus second-order CI (Konowalow and Lengsfield 1987).

Table 4. Molecular Constants for the $a^3\Sigma_u^+$, $b^3\Pi_g$, and $F^1\Pi_u$ Electronic States[a]

Property	$a^3\Sigma_u^+$	$b^3\Pi_g$	$F^1\Pi_u$
r_e Theory	1.0493	1.0681	1.0869
Exp.	1.0457	1.0635	1.0849
T_e[b]	143,768.	148,962.	165,665.
	144,048.	148,835.	165,971.
		(5,194.)	(21,897.)
		(4,787.)	(21,923.)
ω_e[c]	1,816.	1,766.	1,673.
	1,809.	1,769.	1,671.
D_e[d]	15,636.	19,942.	5,293.
	15,806.		

[a] All distances in angstroms and energies in cm-1. Experimental data from Huber and Herzberg (1979).

[b] The first set of values are T_e with respect to the $X^1\Sigma_g^+$ at R=40 au, and the parenthetical values are T_e's with respect to the E_e of $a^3\Sigma_u^+$.

[c] Theoretical ω_e's from $\Delta G(2\text{-}1) - \Delta G(1\text{-}0) = -2\omega_e x_e$ and $\omega_e = G(1\text{-}0) + 2\omega_e x_e$. See Herzberg (1950), pg. 95.

[d] Determined from the energy difference between r_e and R=40 au.

Table 5. Results from Vibrational Analyses of the $a^3\Sigma_u^+$, $b^3\Pi_g$, and $F^1\Pi_u$ States with Energies in cm^{-1} and Lifetimes, τ, in Seconds

v	$a^3\Sigma_u^+$ Energy	τ	$b^3\Pi_g$ Energy	$F^1\Pi_u$ Energy
0	899	18	873	826
1	2,635	15	2,570	2,420
2	4,290	13	4,199	3,936
3	5,867	12	5,757	5,270
4	7,373	11	7,242	
5	8,785	9.6	8,658	
6	10,097	8.5	10,000	
7	11,306	7.5	11,270	
8	12,433	6.7	12,459	
9	13,452	6.0	13,569	

Table 6. The Total Electric Transition Dipole Moment $\mu_1(a^3\Sigma_u^+, X^1\Sigma_g^+)$, for $a^3\Sigma_u^+ \rightarrow X^1\Sigma_g^+$ as a Function R(He-He) (in atomic units).

R(He-He)	$\langle X^1\Sigma_g^+ \vert \mu_{+1} \vert a^3\Sigma_u^+ \rangle$ (x10**6) au
1.30	-3.276
1.50	1.030
1.60	2.046
1.70	2.906
1.85	3.622
2.00	4.058
2.10	4,269
2.15	4.352
2.30	4.557
2.40	4.670
2.50	4.794
2.60	4.868
2.70	4.959
2.85	5.089
3.00	5.340
3.25	5.615
3.50	5.877
4.00	5.990
4.25	5.768
4.50	5.383
4.75	4.882
5.00	4.319
5.50	3.182
6.00	2.199
6.50	1.466
10.00	2.145(-3)*
40.00	5.400(-5)

* Characteristic base ten noted parenthetically.

INTENTIONALLY LEFT BLANK.

6. REFERENCES

Bethe, H. A., and E. E. Salpeter. Quantum Mechanics of One- and Two-Electron Atoms. New York: Plenum, 1977.

Brown, C. M., and M. L. Ginter. J. Mol. Spectroscopic. Vol. 40, p. 302, 1971.

Browne, J. C. Phys. Rev., A 138, p. 9, 1965.

Brutschy, B., and H. Haberland. Phys. Rev., Vol. 19, p. 2,232, 1979.

Calvani, P., B. Maraviglia, and C. Messana. Phys. Lett., Vol. 39A, p. 123, 1972.

Diffenderfer, R. N., and D. R. Yarkony. J. Phys. Chem., Vol. 86, p. 5,098, 1982.

Ginter, M. L., and R. Battino. J. Chem. Phys., Vol. 52, p. 4,469, 1970.

Guberman, S. L., and W. A. Goddard III. Phys. Rev., Vol. A4, p. 1,203, 1975.

Gupta, B. K., and F. A. Matsen. J. Chem. Phys., Vol. 50, p. 3,797, 1969.

Hansen, J. P., and E. L. Pollock. Phys. Rev., Vol. A5, p. 2,214, 1972.

Herzberg, G. Spectra of Diatomic Molecules. New York: Van Nostrand-Rheinhold, 1950.

Huber, K. P., and G. Herzberg. Molecular Spectra and Molecular Structure. New York: Van Nostrand-Rheinhold, 1979.

Jordan, R. M., H. R. Siddiqui, and P. E. Siska. J. Chem. Phys., Vol. 84, p. 6,719, 1986.

Konowalow, D. D., and B. H. Lengsfield III. Chem. Phys. Lett., Vol. 139, p. 417, 1987a.

Konowalow, D. D., and B. H. Lengsfield III. J. Chem. Phys., Vol. 87, p. 4,000, 1987b.

Lengsfield, B. H. J. Chem. Phys., Vol. 73, p. 382, 1980.

Liu, B., and M. Yoshimine. J. Chem. Phys., Vol. 74, p. 612, 1981.

Lundlum, K. H., and L. P. Larson, and J. M. Caffrey. J. Chem. Phys., Vol. 46, p. 127, 1967.

Mehrotra, R., E. K. Mann, and A. J. Dahm. J. Low Temp Phys., Vol. 36, p. 47, 1979.

Mitchell, R. P., and G. W. Rayfield. Phys. Lett., Vol. 37A, p. 231, 1971.

Mulliken, R. S. J. Am. Chem. Soc., Vol. 88, p. 1,849, 1966.

Mulliken, R. S. J. Am. Chem. Soc., Vol. 86, p. 3,183, 1964a.

Mulliken, R. S. Phys. Rev., Vol. A136, p. 962, 1964b.

Peach, G. J. Phys., Vol. B11, p. 2,107, 1978.

Pople, J. A., R. Krishnan, H. B. Schlegel, and J. S. Binckley. Int. J. Quantum Chem., Vol. 13, p. 225, 1979.

Rayfield, G. W. Phys. Rev. Lett., Vol. 23, p. 687, 1969.

Sunil, K. K., J. Lin, H. Siddiqui, P. E. Siska, K. D. Jordan, and R. Shepard. J. Chem. Phys., Vol. 78, p. 6,190, 1983.

Surko, C. M., and F. Reif. Phys. Rev. Lett., Vol. 20, p. 582, 1968a.

Surko, C. M., and F. Reif. Phys. Rev., Vol. 175, p. 229, 1968b.

van Dishoeck, E. F., and A. Dalgarno. J. Chem. Phys., Vol. 79, p. 873, 1983.

van Dishoeck, E. F., S. R. Langhoff, and A. Dalgarno. J. Chem. Phys., Vol. 78, p. 4,552, 1983.

Yarkony, D. R. J. Chem. Phys., Vol. 86, p. 1,642, 1987.

Yarkony, D. R. J. Chem. Phys., Vol. 85, p. 7,261, 1986, and references therein.

No. of Copies	Organization
2	Administrator Defense Technical Info Center ATTN: DTIC-DDA Cameron Station Alexandria, VA 22304-6145
1	HQDA (SARD-TR) WASH DC 20310-0001
1	Commander US Army Materiel Command ATTN: AMCDRA-ST 5001 Eisenhower Avenue Alexandria, VA 22333-0001
1	Commander US Army Laboratory Command ATTN: AMSLC-DL Adelphi, MD 20783-1145
2	Commander US Army, ARDEC ATTN: SMCAR-IMI-I Picatinny Arsenal, NJ 07806-5000
2	Commander US Army, ARDEC ATTN: SMCAR-TDC Picatinny Arsenal, NJ 07806-5000
1	Director Benet Weapons Laboratory US Army, ARDEC ATTN: SMCAR-CCB-TL Watervliet, NY 12189-4050
1	Commander US Army Armament, Munitions and Chemical Command ATTN: SMCAR-ESP-L Rock Island, IL 61299-5000
1	Commander US Army Aviation Systems Command ATTN: AMSAV-DACL 4300 Goodfellow Blvd. St. Louis, MO 63120-1798
1	Director US Army Aviation Research and Technology Activity
1	ATTN: SAVRT-R (Library) M/S 219-3 Ames Research Center Moffett Field, CA 94035-1000

No. of Copies	Organization
1	Commander US Army Missile Command ATTN: AMSMI-RD-CS-R (DOC) Redstone Arsenal, AL 35898-5010
1	Commander US Army Tank-Automotive Command ATTN: AMSTA-TSL (Technical Library) Warren, MI 48397-5000
1	Director US Army TRADOC Analysis Command ATTN: ATAA-SL White Sands Missile Range, NM 88002-5502
(Class. only) 1	Commandant US Army Infantry School ATTN: ATSH-CD (Security Mgr.) Fort Benning, GA 31905-5660
(Unclass. only) 1	Commandant US Army Infantry School ATTN: ATSH-CD-CSO-OR Fort Benning, GA 31905-5660
1	Air Force Armament Laboratory ATTN: AFATL/DLODL Eglin AFB, FL 32542-5000

Aberdeen Proving Ground

No. of Copies	Organization
2	Dir, USAMSAA ATTN: AMXSY-D AMXSY-MP, H. Cohen
1	Cdr, USATECOM ATTN: AMSTE-TO-F
3	Cdr, CRDEC, AMCCOM ATTN: SMCCR-RSP-A SMCCR-MU SMCCR-MSI
1	Dir, VLAMO ATTN: AMSLC-VL-D

No. of Copies	Organization
4	Commander US Army Research Office ATTN: R. Ghirardelli D. Mann R. Singleton R. Shaw P.O. Box 12211 Research Triangle Park, NC 27709-2211
2	Commander US Army, ARDEC ATTN: SMCAR-AEE-B, D.S. Downs SMCAR-AEE, J.A. Lannon Picatinny Arsenal, NJ 07806-5000
1	Commander US Army, ARDEC ATTN: SMCAR-AEE-BR, L. Harris Picatinny Arsenal, NJ 07806-5000
2	Commander US Army Missile Command ATTN: AMSMI-RK, D.J. Ifshin W. Wharton Redstone Arsenal, AL 35898
1	Commander US Army Missile Command ATTN: AMSMI-RKA, A.R. Maykut Redstone Arsenal, AL 35898-5249
1	Office of Naval Research Department of the Navy ATTN: R.S. Miller, Code 432 800 N. Quincy Street Arlington, VA 22217
1	Commander Naval Air Systems Command ATTN: J. Ramnarace, AIR-54111C Washington, DC 20360
1	Commander Naval Surface Warfare Center ATTN: J.L. East, Jr., G-23 Dahlgren, VA 22448-5000
2	Commander Naval Surface Warfare Center ATTN: R. Bernecker, R-13 G.B. Wilmot, R-16 Silver Spring, MD 20903-5000

No. of Copies	Organization
5	Commander Naval Research Laboratory ATTN: M.C. Lin J. McDonald E. Oran J. Shnur R.J. Doyle, Code 6110 Washington, DC 20375
1	Commanding Officer Naval Underwater Systems Center Weapons Dept. ATTN: R.S. Lazar/Code 36301 Newport, RI 02840
2	Commander Naval Weapons Center ATTN: T. Boggs, Code 388 T. Parr, Code 3895 China Lake, CA 93555-6001
1	Superintendent Naval Postgraduate School Dept. of Aeronautics ATTN: D.W. Netzer Monterey, CA 93940
3	AL/LSCF ATTN: R. Corley R. Geisler J. Levine Edwards AFB, CA 93523-5000
1	AL/MKPB ATTN: B. Goshgarian Edwards AFB, CA 93523-5000
1	AFOSR ATTN: J.M. Tishkoff Bolling Air Force Base Washington, DC 20332
1	OSD/SDIO/IST ATTN: L. Caveny Pentagon Washington, DC 20301-7100
1	Commandant USAFAS ATTN: ATSF-TSM-CN Fort Sill, OK 73503-5600
1	F.J. Seiler ATTN: S.A. Shackleford USAF Academy, CO 80840-6528

No. of Copies	Organization
1	University of Dayton Research Institute ATTN: D. Campbell AL/PAP Edwards AFB, CA 93523
1	NASA Langley Research Center Langley Station ATTN: G.B. Northam/MS 168 Hampton, VA 23365
4	National Bureau of Standards ATTN: J. Hastie M. Jacox T. Kashiwagi H. Semerjian US Department of Commerce Washington, DC 20234
1	Aerojet Solid Propulsion Co. ATTN: P. Micheli Sacramento, GA 95813
1	Applied Combustion Technology, Inc. ATTN: A.M. Varney P.O. Box 607885 Orlando, FL 32860
2	Applied Mechanics Reviews The American Society of Mechanical Engineers ATTN: R.E. White A.B. Wenzel 345 E. 47th Street New York, NY 10017
1	Atlantic Research Corp. ATTN: M.K. King 5390 Cherokee Avenue Alexandria, VA 22314
1	Atlantic Research Corp. ATTN: R.H.W. Waesche 7511 Wellington Road Gainesville, VA 22065
1	AVCO Everett Research Laboratory Division ATTN: D. Stickler 2385 Revere Beach Parkway Everett, MA 02149

No. of Copies	Organization
1	Battelle Memorial Institute Tactical Technology Center ATTN: J. Huggins 505 King Avenue Columbus, OH 43201
1	Cohen Professional Services ATTN: N.S. Cohen 141 Channing Street Redlands, CA 92373
1	Exxon Research & Eng. Co. ATTN: A. Dean Route 22E Annandale, NJ 08801
1	Ford Aerospace and Communications Corp. DIVAD Division Div. Hq., Irvine ATTN: D. Williams Main Street & Ford Road Newport Beach, CA 92663
1	General Applied Science Laboratories, Inc. 77 Raynor Avenue Ronkonkama, NY 11779-6649
1	General Electric Ordnance Systems ATTN: J. Mandzy 100 Plastics Avenue Pittsfield, MA 01203
2	General Motors Rsch Labs Physics Department ATTN: T. Sloan R. Teets Warren, MI 48090
2	Hercules, Inc. Allegheny Ballistics Lab. ATTN: W.B. Walkup E.A. Yount P.O. Box 210 Rocket Center, WV 26726
1	Honeywell, Inc. Government and Aerospace Products ATTN: D.E. Broden/ MS MN50-2000 600 2nd Street NE Hopkins, MN 55343

No. of Copies	Organization
1	Honeywell, Inc. ATTN: R.E. Tompkins MN38-3300 10400 Yellow Circle Drive Minnetonka, MN 55343
1	IBM Corporation ATTN: A.C. Tam Research Division 5600 Cottle Road San Jose, CA 95193
1	IIT Research Institute ATTN: R.F. Remaly 10 West 35th Street Chicago, IL 60616
2	Director Lawrence Livermore National Laboratory ATTN: C. Westbrook M. Costantino P.O. Box 808 Livermore, CA 94550
1	Lockheed Missiles & Space Co. ATTN: George Lo 3251 Hanover Street Dept. 52-35/B204/2 Palo Alto, CA 94304
1	Los Alamos National Lab ATTN: B. Nichols T7, MS-B284 P.O. Box 1663 Los Alamos, NM 87545
1	National Science Foundation ATTN: A.B. Harvey Washington, DC 20550
1	Olin Ordnance ATTN: V. McDonald, Library P.O. Box 222 St. Marks, FL 32355-0222
1	Paul Gough Associates, Inc. ATTN: P.S. Gough 1048 South Street Portsmouth, NH 03801-5423

No. of Copies	Organization
2	Princeton Combustion Research Laboratories, Inc. ATTN: M. Summerfield N.A. Messina 475 US Highway One Monmouth Junction, NJ 08852
1	Hughes Aircraft Company ATTN: T.E. Ward 8433 Fallbrook Avenue Canoga Park, CA 91303
1	Rockwell International Corp. Rocketdyne Division ATTN: J.E. Flanagan/HB02 6633 Canoga Avenue Canoga Park, CA 91304
4	Sandia National Laboratories Division 8354 ATTN: R. Cattolica S. Johnston P. Mattern D. Stephenson Livermore, CA 94550
1	Science Applications, Inc. ATTN: R.B. Edelman 23146 Cumorah Crest Woodland Hills, CA 91364
3	SRI International ATTN: G. Smith D. Crosley D. Golden 333 Ravenswood Avenue Menlo Park, CA 94025
1	Stevens Institute of Tech. Davidson Laboratory ATTN: R. McAlevy, III Hoboken, NJ 07030
1	Sverdrup Technology, Inc. LERC Group ATTN: R.J. Locke, MS SVR-2 2001 Aerospace Parkway Brook Park, OH 44142
1	Thiokol Corporation Elkton Division ATTN: S.F. Palopoli P.O. Box 241 Elkton, MD 21921

No. of Copies	Organization
1	Morton Thiokol, Inc. Huntsville Division ATTN: J. Deur Huntsville, AL 35807-7501
3	Thiokol Corporation Wasatch Division ATTN: S.J. Bennett P.O. Box 524 Brigham City, UT 84302
1	United Technologies Research Center ATTN: A.C. Eckbreth East Hartford, CT 06108
3	United Technologies Corp. Chemical Systems Division ATTN: R.S. Brown T.D. Myers (2 copies) P.O. Box 49028 San Jose, CA 95161-9028
1	Universal Propulsion Company ATTN: H.J. McSpadden Black Canyon Stage 1 Box 1140 Phoenix, AZ 85029
1	Veritay Technology, Inc. ATTN: E.B. Fisher 4845 Millersport Highway P.O. Box 305 East Amherst, NY 14051-0305
1	Brigham Young University Dept. of Chemical Engineering ATTN: M.W. Beckstead Provo, UT 84058
1	California Institute of Tech. Jet Propulsion Laboratory ATTN: L. Strand/MS 512/102 4800 Oak Grove Drive Pasadena, CA 91009
1	California Institute of Technology ATTN: F.E.C. Culick/ MC 301-46 204 Karman Lab. Pasadena, CA 91125
1	University of California Los Alamos Scientific Lab. P.O. Box 1663, Mail Stop B216 Los Alamos, NM 87545

No. of Copies	Organization
1	University of California, Berkeley Chemistry Deparment ATTN: C. Bradley Moore 211 Lewis Hall Berkeley, CA 94720
1	University of California, San Diego ATTN: F.A. Williams AMES, B010 La Jolla, CA 92093
2	University of California, Santa Barbara Quantum Institute ATTN: K. Schofield M. Steinberg Santa Barbara, CA 93106
1	University of Colorado at Boulder Engineering Center ATTN: J. Daily Campus Box 427 Boulder, CO 80309-0427
2	University of Southern California Dept. of Chemistry ATTN: S. Benson C. Wittig Los Angeles, CA 90007
1	Case Western Reserve Univ. Div. of Aerospace Sciences ATTN: J. Tien Cleveland, OH 44135
1	Cornell University Department of Chemistry ATTN: T.A. Cool Baker Laboratory Ithaca, NY 14853
1	University of Delaware ATTN: T. Brill Chemistry Department Newark, DE 19711
1	University of Florida Dept. of Chemistry ATTN: J. Winefordner Gainesville, FL 32611

No. of Copies	Organization
3	Georgia Institute of Technology School of Aerospace Engineering ATTN: E. Price W.C. Strahle B.T. Zinn Atlanta, GA 30332
1	University of Illinois Dept. of Mech. Eng. ATTN: H. Krier 144MEB, 1206 W. Green St. Urbana, IL 61801
1	Johns Hopkins University/APL Chemical Propulsion Information Agency ATTN: T.W. Christian Johns Hopkins Road Laurel, MD 20707
1	University of Michigan Gas Dynamics Lab Aerospace Engineering Bldg. ATTN: G.M. Faeth Ann Arbor, MI 48109-2140
1	University of Minnesota Dept. of Mechanical Engineering ATTN: E. Fletcher Minneapolis, MN 55455
3	Pennsylvania State University Applied Research Laboratory ATTN: K.K. Kuo H. Palmer M. Micci University Park, PA 16802
1	Pennsylvania State University Dept. of Mechanical Engineering ATTN: V. Yang University Park, PA 16802
1	Polytechnic Institute of NY Graduate Center ATTN: S. Lederman Route 110 Farmingdale, NY 11735

No. of Copies	Organization
2	Princeton University Forrestal Campus Library ATTN: K. Brezinsky I. Glassman P.O. Box 710 Princeton, NJ 08540
1	Purdue University School of Aeronautics and Astronautics ATTN: J.R. Osborn Grissom Hall West Lafayette, IN 47906
1	Purdue University Department of Chemistry ATTN: E. Grant West Lafayette, IN 47906
2	Purdue University School of Mechanical Engineering ATTN: N.M. Laurendeau S.N.B. Murthy TSPC Chaffee Hall West Lafayette, IN 47906
1	Rensselaer Polytechnic Inst. Dept. of Chemical Engineering ATTN: A. Fontijn Troy, NY 12181
1	Stanford University Dept. of Mechanical Engineering ATTN: R. Hanson Stanford, CA 94305
1	University of Texas Dept. of Chemistry ATTN: W. Gardiner Austin, TX 78712
1	University of Utah Dept. of Chemical Engineering ATTN: G. Flandro Salt Lake City, UT 84112
1	Virginia Polytechnic Institute and State University ATTN: J.A. Schetz Blacksburg, VA 24061

No. of Copies	Organization
1	Freedman Associates ATTN: E. Freedman 2411 Diana Road Baltimore, MD 21209-1525

USER EVALUATION SHEET/CHANGE OF ADDRESS

This Laboratory undertakes a continuing effort to improve the quality of the reports it publishes. Your comments/answers to the items/questions below will aid us in our efforts.

1. BRL Report Number BRL-TR-3184 Date of Report DECEMBER 1990

2. Date Report Received ______________________

3. Does this report satisfy a need? (Comment on purpose, related project, or other area of interest for which the report will be used.) ______________________

4. Specifically, how is the report being used? (Information source, design data, procedure, source of ideas, etc.) ______________________

5. Has the information in this report led to any quantitative savings as far as man-hours or dollars saved, operating costs avoided, or efficiencies achieved, etc? If so, please elaborate. ______________________

6. General Comments. What do you think should be changed to improve future reports? (Indicate changes to organization, technical content, format, etc.) ______________________

CURRENT ADDRESS

Name

Organization

Address

City, State, Zip Code

7. If indicating a Change of Address or Address Correction, please provide the New or Correct Address in Block 6 above and the Old or Incorrect address below.

OLD ADDRESS

Name

Organization

Address

City, State, Zip Code

(Remove this sheet, fold as indicated, staple or tape closed, and mail.)

--FOLD HERE--

DEPARTMENT OF THE ARMY

Director
U.S. Army Ballistic Research Laboratory
ATTN: SLCBR-DD-T
Aberdeen Proving Ground, MD 2100 -5066

OFFICIAL BUSINESS

NO POSTAGE NECESSARY IF MAILED IN THE UNITED STATES

BUSINESS REPLY MAIL
FIRST CLASS PERMIT No 0001, APG, MD

POSTAGE WILL BE PAID BY ADDRESSEE

Director
U.S. Army Ballistic Research Laboratory
ATTN: SLCBR-DD-T
Aberdeen Proving Ground, MD 21005-9989

--FOLD HERE--